THE ASTROPHYSICAL JOURNAL, 436:586–598, 1994 December 1

MULTIWAVELENGTH TESTS OF THE DUSTY TORUS MODEL FOR SEYFERT GALAXIES

JOHN S. MULCHAEY,[1,2] ANURADHA KORATKAR,[1] MARTIN J. WARD,[3] ANDREW S. WILSON,[1,2]
MARK WHITTLE,[4] ROBERT R. J. ANTONUCCI,[5] ANNE L. KINNEY,[1] AND TODD HURT[5]
Received 1994 January 31; accepted 1994 May 31

ABSTRACT

We present a compilation of emission properties for a sample of 116 Seyfert galaxies based on both previously unpublished data and measurements available in the literature. These measurements include fluxes in the emission lines [O III] λ5007 and Hβ, as well as the infrared (25–60 μm), ultraviolet (1450 Å), soft (0.2–4 keV), and hard (2–10 keV) X-ray continua. These data are used to try to distinguish between isotropic and anisotropic emission properties of Seyfert galaxies. The distribution functions of [O III] λ5007, infrared, and hard X-ray continuum are similar for Seyfert 1's and Seyfert 2's, consistent with these properties being isotropic. The ultraviolet and soft X-ray continua of Seyfert 2's are underluminous relative to the type 1's suggesting photons at these energies escape from the central source anisotropically. There is a correlation between the ultraviolet continuum and emission-line fluxes in Seyfert 1's consistent with the idea that the central engine is responsible for powering the line emission. No such correlation is found for the Seyfert 2's. Instead, the scatter in the plot of ultraviolet continuum versus line emission suggests the true nuclear continuum luminosity is not seen at Earth in these objects. These properties are consistent with those expected in the dusty torus model.

Subject headings: galaxies: active — galaxies: nuclei — galaxies: Seyfert — infrared: galaxies — ultraviolet: galaxies — X-rays: galaxies

1. INTRODUCTION

One of the goals of active galactic nuclei (AGNs) research is to understand the relationship, if any, between the various members of the AGNs family. A major effort toward meeting this goal has come from the consideration of unified schemes (see Antonucci 1993). In these models, the observed differences between broad and narrow emission-line active galaxies are due to obscuration and viewing angle effects and not to intrinsic, physical differences. The unified models simplify the taxonomy of AGNs and thus the task of finding physical models to describe them.

The discovery by Antonucci & Miller (1985) of a Seyfert 1 spectrum in the polarized light of the Seyfert 2 galaxy NGC 1068 provided a breakthrough in our understanding of nearby, radio-quiet AGNs. Using spectropolarimetry, they found broad Balmer lines and Fe II emission characteristic of a Seyfert 1 spectrum. Antonucci & Miller proposed that NGC 1068 contains a broad line region (BLR) and a nonstellar continuum source which are blocked from our view by an optically and geometrically thick torus. In the model, these components, hidden from our direct view, are visible only through scattering by an optically thin cloud of electrons along the torus axis. For several other Seyfert 2's, the evidence is strong that they too contain "hidden" Seyfert 1 nuclei. In particular, spectropolarimetry has revealed broad lines in eight more Seyfert 2's (Miller & Goodrich 1990; Tran, Miller, & Kay 1992), suggesting the model may apply to many, or even all, Seyfert galaxies.

In the dusty torus model, the optical, ultraviolet, and perhaps soft X-ray radiation is expected to be collimated by the torus and thus escape anisotropically. There is now compelling evidence that this is true in at least some objects. Imaging in optical emission lines shows that the narrow line region (NLR) is preferentially elongated along the radio axis (Haniff, Wilson, & Ward 1988) and has a similar spatial scale. In some cases, these images show a conical or biconical morphology (e.g., Pogge 1989; Tadhunter & Tsvetanov 1989; Evans et al. 1991; Storchi-Bergmann, Wilson, & Baldwin 1992b). These "ionization cones" are direct evidence that the ionizing photons escape in a cone around the radio axis. Energetic arguments also indicate the gas in the NLR of some Seyfert 2's sees a more intense radiation field than we infer from Earth, suggesting collimation of the ionizing photons (Wilson, Ward, & Haniff 1988; Penston et al. 1990; Kinney et al. 1991a). This collimation could result from either shadowing of an intrinsically isotropic source or an intrinsically anisotropic emitter (Madau 1988; Acosta-Pulido et al. 1990).

While most of the ionizing radiation is expected to escape anisotropically, energy emitted at both higher (i.e., hard X-rays, gamma rays) and lower frequencies (i.e., radio, infrared) may be able to penetrate the torus and escape isotropically. In addition, any emission produced on scales larger than the torus should be free of viewing angle effects and thus seen in similar strengths in Seyfert 1's and 2's. Possible isotropic properties include optical emission lines produced in the NLR (i.e., [O III] λ5007, etc.) and radio, infrared, and hard X-ray continuum emission. Over the last decade there have been several attempts to determine which, if any, of these properties are truly isotropic. While the nuclear radio sources of the well-studied Seyfert 2's tend to be stronger than the best studied type 1's (Ulvestad & Wilson 1984), this result could be due to a selection effect, since the famous Seyfert 2's were discovered by

[1] Space Telescope Science Institute, 3700 San Martin Drive, Baltimore, MD 21218.
[2] Astronomy Department, University of Maryland, College Park, MD 20742.
[3] Department of Astrophysics, University of Oxford, Keble Road, Oxford, England, OX1, 3RH, UK.
[4] Astronomy Department, University of Virginia, Charlottesville, VA 22903.
[5] Physics Department, University of California at Santa Barbara, Santa Barbara, CA 93106.

their UV excesses and thus, in the reflection model, represent the high end of the luminosity function (e.g., Lawrence 1987). Dahari & De Robertis (1988) found that the luminosity distributions of the two Seyfert types in the infrared and the emission line [O III] λ5007 were similar (see also a more recent study by Keel et al. 1994), consistent with the unified model. However, they also found that the ratio of 60 μm to [O III] λ5007 flux was different in the two types and suggested Seyfert 2's were on average more dusty. The luminosity of the Seyfert 2's detected to date in the hard (2–10 keV) X-ray band are within the range that is typical for Seyfert 1's (Awaki et al. 1991), although the failure to detect the Seyfert 2 counterparts to the very X-ray luminous ($L_{2-10\,\mathrm{keV}} \sim 10^{45}$ ergs s^{-1}) Seyfert 1's may be a problem for the simplest of unified schemes (Mulchaey, Mushotzky, & Weaver 1992). Thus, none of these properties has firmly been established as an isotropic quantity.

While it seems likely that at least some Seyfert 2's harbor buried Seyfert 1 nuclei, the applicability of the model to all objects is not yet known. It is possible that there are really two types of Seyfert 2's, "hidden" Seyfert 1's and "true" Seyfert 2's. The "true" Seyfert 2's would contain no BLR and a weak nonstellar continuum compared to Seyfert 1's. Evidence for a bimodal distribution for Seyfert 2's in at least one emission property would lend support to the idea of two Seyfert 2 populations. In the last decade, space-based telescopes have provided a wealth of new information in the previously unexplored infrared, ultraviolet, and X-ray wavelengths. The purpose of the present paper is to examine the emission in these bandpasses and combine it with existing optical emission-line data to search for evidence of two different Seyfert 2 populations and make direct comparisons with the type 1 objects. In the next section, we define the sample used for this study. Section 3 contains a detailed description of the sources of our data and of the analysis methods used. Comparisons of the emission properties of the two Seyfert types are given in § 4 with an emphasis on the interpretation within the context of the dusty torus model. A summary is provided in § 5.

2. SAMPLE SELECTION

We adopted the 140 Seyfert galaxies in Whittle (1992) as our starting sample. However, since so few Seyfert 2's have available spectra in the hard (2–10 keV) X-ray band, we have supplemented this sample with five other Seyfert 2's for which such data exist. The original sample of Whittle (1992) was defined to include all Seyferts with high to intermediate dispersion measurements of the [O III] λ5007 line width available and thus is a rather heterogeneous group. Ideally, one would prefer to select a sample by one isotropic property and then make comparisons with other properties (e.g., Antonucci 1993). Unfortunately, it is not clear what properties are truly isotropic in Seyfert galaxies. The Whittle (1992) sample has several advantages over other possible samples. It offers the best available compilation of [O III] λ5007 fluxes, because aperture sizes were considered. Second, the Seyfert type (class 1, 2, or intermediate) of each galaxy in the sample has been assigned consistently, based on the presence of a broad emission-line component and the ratio of [O III] λ5007 to Hβ flux. For our purposes, we group activity types 1.2 and 1.5 with Seyfert 1's and types 1.8 and 1.9 with Seyfert 2's. In Table 1, we list the galaxies in our sample that have observations available in at least two of the following bands: infrared (25 μm and 60 μm), [O III] λ5007, ultraviolet (1450 Å), soft X-ray (0.5–0.4 keV), and hard X-ray (2–10 keV). Our final sample contains 116 galaxies.

3. DATA

3.1. *Infrared*

All infrared fluxes used are based on *IRAS* data. These fluxes are taken from the *IRAS* Point Source Catalog, the *IRAS* Faint Source Survey (FSS) or, where available, co-added fluxes from multiple *IRAS* scans. For this paper, we adopt the following definition of infrared flux:

$$F(\mathrm{IR}) = S_{25\,\mu\mathrm{m}} \times (\nu_{25\,\mu\mathrm{m}}) + S_{60\,\mu\mathrm{m}} \times (\nu_{60\,\mu\mathrm{m}}) ,$$

where S_λ is the flux density at wavelength λ. This definition of IR flux has the advantage that most of the sample objects are detected at these two wavelengths, while at 12 and 100 μm the data are more incomplete.

3.2. *Optical Emission Lines*

All optical emission-line fluxes are taken from Whittle (1992), except where noted in Table 1. The flux in Hβ is the total observed flux (broad plus narrow component). The narrow-line Balmer decrement can be used to estimate the reddening to the NLR (e.g., Osterbrock 1989). However, for Seyfert 1's, this procedure requires deblending the narrow component from the broad one and is thus somewhat model-dependent. For this reason, we have not applied a reddening correction to the observed line fluxes. The narrow-line Balmer decrement is given in column (2) of Table 1 when such data are available, as a reminder that for a few objects the line fluxes may be significantly underestimated (e.g., IC 4329A, NGC 7314, Mrk 622, ESO 103-G35). Reddening of the NLR gas may produce scatter in our comparisons with other emission properties.

3.3. *Ultraviolet (UV)*

Previously published ultraviolet fluxes of Seyfert galaxies have been largely restricted to *IUE* observations of type 1 objects. However, the development of slit-weighted extraction techniques for *IUE* data (Kinney, Bohlin, & Neill 1991b) allows estimates of the ultraviolet continuum in many more Seyfert 2 galaxies. While Kinney et al. (1991a), Kinney et al. (1993), and Masse-Hess et al. (1994) include fluxes for many of the brighter Seyfert 2's, many objects observed with *IUE* do not have published data. To get a statistically significant sample, we obtained ultraviolet data for all of our sample objects in the *IUE* archive and estimated continuum fluxes whenever possible. The flux was estimated by averaging the continuum in a 100 Å wide band centered on rest wavelength 1450 Å. Table 1 contains a UV continuum flux measurement for approximately a dozen Seyfert 2's that have no previous published value, nearly doubling the sample of type 2 objects with such a measurement. No reddening correction has been applied to the fluxes. Kinney et al. (1991a) have shown that the slopes of the ultraviolet continua in Seyfert 2's are indistinguishable from those of Seyfert 1's, with a relatively small spread among those objects with good data. This suggests the ultraviolet continua in Seyfert 2 galaxies are not highly reddened.

3.4. *Soft X-Rays (SX) (0.2–4* keV)

Many Seyfert galaxies were observed with the *Einstein Observatory*, producing the largest SX database available. The most complete study to date is that of Kruper, Urry, & Canizares (1990), and the majority of the SX fluxes listed in Table 1 are taken from this source. A handful of other objects were

TABLE 1A

SEYFERT 1 GALAXIES

Galaxy (1)	Hα/Hβ (2)	log (IR) (3)	log ([O III]) (4)	log (Hβ) (5)	log (UV) (6)	log (SX) (7)	log (HX) (8)	References (Hα/Hβ) (9)	References (HX) (10)
NGC 1566	5.0	−10.0	−12.52	−12.74	−14.31	−11.15	...	1	
NGC 3227	5.75	−9.51	−12.19	−12.60	−13.72	−10.87	−10.31	1	7
NGC 3516	4.9	−10.04	−12.32	−12.14	−13.98	−11.40	−10.61	2	8
NGC 3783	3.7	−9.67	−11.89	−11.89	−13.38	−10.52	−10.29	3	9
NGC 4051	3.2	−9.42	−12.41	−12.60	−13.93	−10.66	−11.48	4	10
NGC 4151	3.1	−9.39	−10.94	−11.35	−13.14	−11.01	−10.05	5	11
NGC 4235	...	−10.73	−13.62	−13.18	...	−11.44	...		
NGC 4593	4.6	−9.92	−12.76	−12.19	−13.89	−10.51	−10.67	2	9
NGC 5548	4.2	−10.17	−12.24	−12.08	−13.31	−10.44	−10.37	1	12
NGC 6814	...	−9.76	−12.87	−13.36	−14.75	−11.69	...		9
NGC 7469	9.33	−8.99	−12.24	−12.00	−13.24	−10.53	−10.39	1	13
NGC 7603	...	< −10.46	−13.32	−13.13	−14.11	−11.27			
Mrk 6	...	−10.18	−12.12	−12.49	< −14.29	...			
Mrk 9	...	−10.37	−12.96	−12.72	−13.59	−11.37			
Mrk 10	...	−10.49	−12.85	−12.72	−14.01	...			
Mrk 42	...	< −10.81	−13.91	−13.43	−14.50	...			
Mrk 79	3.8	−10.11	−12.43	−12.26	−13.75	−10.71	−10.61	2	9
Mrk 124	...	−10.50	−13.19	−12.96	...	...			
Mrk 141	5.01	−10.56	−13.41	−13.15	...	...	...	1	
Mrk 142	...	...	−13.72	−13.14	−13.91				
Mrk 279	...	−10.19	−12.85	−12.47	−13.42	−10.63			
Mrk 290	...	< −10.93	−12.62	−12.48	−13.61	−10.81			
Mrk 304	...	...	−13.24	−12.44	−14.07	−12.02			
Mrk 315	6.5	−10.27	−13.17	−13.20	...	−12.02	...	2	
Mrk 335	...	−10.55	−12.64	−12.02	−13.13	...	−11.07		12
Mrk 352	...	...	−13.31	−12.66	−13.80	−10.48			
Mrk 359	5.25	−10.29	−12.96	−13.46	−13.85	−10.09	...	1	
Mrk 372	...	−10.78	−12.89	−13.00	−13.86	−12.06			
Mrk 474	...	−10.21	−13.32	−13.21	...	− 9.30			
Mrk 486	...	...	−13.09	−12.44	−14.34	...			
Mrk 506	2.85	...	−12.89	−13.24	−13.90	−11.15	...	2	
Mrk 509	< 1.5	−10.15	−12.09	−11.78	−13.00	...	−10.35	6	9
Mrk 590	...	−10.62	−13.28	−13.22	−14.14	−10.67	−10.53		9
Mrk 618	...	−9.96	−12.89	−12.66	...	−11.04			
Mrk 704	8.7	−10.43	−12.89	−12.59	−14.04	−11.01	...	1	
Mrk 734	...	−10.54	−13.05	−12.96	...	−12.57			
Mrk 766	5.1	−9.77	−12.17	−12.74	−14.20	−10.79	...	5	
Mrk 817	3.6	−9.94	−12.89	−12.40	−13.46	...	...	2	
Mrk 871	...	−10.47	−13.26	−12.96					
Mrk 915	...	−10.52	−12.34	−12.96					
Mrk 975	...	−10.40	−12.77	−12.74					
Mrk 1018	6.92	...	−13.47	−13.92	−13.92	...	...	1	
Mrk 1040	...	−9.87	−12.89	−12.85	...	−10.98	−10.70		9
Mrk 1048	...	−10.20	−12.68	−12.59	−13.85	−10.79			
Mrk 1152	...	...	−13.39	−13.31	−14.94				
Mrk 1239	...	−10.03	−12.64	−12.77					
Mrk 1388	5.13	−10.78	−12.59	−13.62	−14.79			1	
AKN 120	...	−10.42	−13.03	−11.77	−13.30	−10.57	−10.46		9
AKN 202	...	−10.58	−13.05	−12.55					
AKN 564	...	−10.30	−12.72	−12.72	−13.88				
IC 4329A	11.5	−9.78	−12.47	−12.19	< −14.41	−10.31	− 9.93	2	9
II Zw 136	...	−10.51	−12.74	−12.32	−13.18	−11.15			
MCG −2-58-22	...	...	−12.46	−12.14	−13.39				
MCG 8-11-11	4.37	−9.75	−12.15	−12.54	−13.38	− 9.53	−10.28	1	9
Fair 9	...	...	−12.62	−11.80	−13.29	−10.24			
Fair 51	...	−10.00	−12.55	−12.49					
ESO 141-G55	...	−10.48	−12.72	−12.15	−13.00	−10.84	−10.50	...	9

NOTES.—Col. (1) Galaxy name; Col. (2) Flux ratio of narrow Hα to narrow Hβ; Col. (3) Logarithm of infrared flux as defined in § 3.1 (ergs s^{-1} cm^{-2}); Col. (4) Logarithm of total [O III] λ5007 flux (ergs s^{-1} cm^{-2}). All fluxes are taken from Whittle (1992), except NGC 1667 (Storchi-Bergmann, Bica, & Pastoriza 1990); Col. (5) Logarithm of total Hβ flux (ergs s^{-1} cm^{-2}). All fluxes are taken from Whittle (1992); Col. (6) Logarithm of total observed *IUE* flux at 1450 Å (ergs s^{-1} cm^{-2} $Å^{-1}$). In cases where more than one *IUE* spectrum was available, the measured flux has been averaged. The flux for NGC 4151 is the average of all *IUE* observations between 1983 and 1990 (Ulrich et al. 1991); Col. (7) Logarithm of total observed *Einstein* flux between 0.2 and 4 keV (ergs s^{-1} cm^{-2}). Fluxes are taken from Kruper et al. (1990), with the exception of NGC 1358, NGC 3281, NGC 4151, NGC 4388, NGC 5135, NGC 5273, NGC 5643, NGC 6890, NGC 7314, IC 4329A, IC 5063, Mrk 1 and Mrk 474 (taken from Fabbiano et al. 1992), Mrk 79, Mrk 198, Mrk 359, Mrk 734, MCG 8-11-11, ESO 141-G55, ESO 103-G35, and TOL 0109-383 (taken from Green, Anderson, & Ward 1992), NGC 1386, NGC 4051, NGC 4593, NGC 5728, NGC 7603, Mrk 34, Mrk 176, Mrk 268, Mrk 270, and Mrk 766 (this paper); Col. (8) Logarithm of total 2–10 keV flux corrected for observed absorption (ergs s^{-1} cm^{-2}).

TABLE 1B

SEYFERT 2 GALAXIES

Galaxy (1)	Hα/Hβ (2)	log (IR) (3)	log ([O III]) (4)	log (Hβ) (5)	log (UV) (6)	log (SX) (7)	log (HX) (8)	References (Hα/Hβ) (9)	References (HX) (10)
NGC 526A	3.0	−10.31	−12.57	−13.68	...	...	−10.56	14	9
NGC 1068	4.47	−8.04	−10.70	−11.77	−13.22	−10.83	−11.31	1	21
NGC 1320	4.86	−9.96	−12.85	−13.85	...			15	
NGC 1358	3.36	−10.80	−12.89	−13.77	...	12.85		16	
NGC 1386	4.87	−9.67	−12.10	−13.28	...	−12.17		16	
NGC 1667	4.31	−9.71	−13.17	...	−14.70		−11.30		22
NGC 2110	8.13	−9.82	−12.77	−13.47	−14.66	−11.48	−10.42	1	9
NGC 2992	7.08	−9.59	−12.04	−13.09	−14.85	−10.56	−10.19	1	9
NGC 3081	4.53	...	−11.90	−13.09	−14.60	−12.09		16	
NGC 3185	...	−10.36	−13.51	−14.22	...				
NGC 3281	6.13	−9.50	−13.26	−14.30	...	< −12.14		16	
NGC 4388	5.89	−9.36	−12.32	−13.42	−14.29	−12.18	−10.68	1	23
NGC 4507	5.02	−9.74	−11.96	−12.94	−14.51	−12.28	−10.19	1	8
NGC 4968	14.9	−9.94	−13.00	−14.40				17	
NGC 5135	6.12	−9.25	−12.66	−13.37	−14.02	−12.47		16	
NGC 5273	3.31	−10.40	−13.66	−14.70	−14.30	−11.98		1	
NGC 5506	7.41	−9.36	−12.35	−13.26	−15.00	−10.72	−10.48	1	9
NGC 5643	6.17	−9.16	−12.10	−13.32	−14.30	−11.98		16	
NGC 5674	...	−10.29	...	...	−14.49	−12.34	−10.96		24
NGC 5728	5.96	−9.56	−12.17	−13.24	−14.44	−12.12		16	
NGC 5929	5.50	−9.50	−13.03	−13.64	...			1	
NGC 6221	8.30	−8.75	−13.21	−13.08	−14.96			18	
NGC 6890	4.17	−9.88	−12.72	−14.05	...	< −12.40		16	
NGC 7172	...	−9.73	...	...	...		−10.18		9
NGC 7212	5.01	−9.94	−12.15	−13.19	...			1	
NGC 7314	20.0	−9.90	−13.21	−14.19	...	< −11.98	−10.53	18	9
NGC 7496	...	−9.52	...	...	...	−12.34	−11.10		24
NGC 7582	8.32	−8.80	−12.46	−12.85	−14.82	−11.43	−10.25	1	9
Mrk 1	5.89	−9.96	−12.22	−13.27	...	< −12.32		1	
Mrk 3	6.61	−9.61	−11.46	−12.54	−14.84	−12.11	−10.37	1	25
Mrk 34	10.47	−10.35	−12.17	−13.24	−14.60	−12.39		1	
Mrk 78	6.46	−10.24	−12.18	−13.30	< −14.64	−12.45		1	
Mrk 176	6.57	−10.52	−12.73	−14.01	...	< −12.51		1	
Mrk 198	3.89	−10.64	−12.90	−13.82	...	< −12.44		1	
Mrk 266	5.89	−9.61	−13.49	−14.17	−14.35			1	
Mrk 268	5.01	−10.30	−13.17	−14.38	...	−12.52		1	
Mrk 270	3.80	−11.00	−12.57	−13.66	−14.91	−12.60		1	
Mrk 273	9.33	−9.16	−12.62	−13.52	< −15.22	−11.77		1	
Mrk 348	6.02	−10.12	−12.38	−13.40	−14.77	−12.44	−10.77	1	26
Mrk 463	5.62	−9.86	−12.14	−12.96	−14.30	−12.71		1	
Mrk 477	5.4	−10.22	−11.82	−12.77	−14.16	−12.14		1	
Mrk 533	5.00	−9.63	−12.31	−13.42	−14.32		−11.08	1	22
Mrk 573	4.17	−10.13	−11.80	−12.89	−14.52	−12.47		1	
Mrk 609	8.91	−9.98	−13.15	−13.40	...			1	
Mrk 612	6.61	−10.36	−12.74	−13.74	...			1	
Mrk 622	18.20	−10.27	−13.40	−14.52	...			1	
Mrk 883	5.01	−10.43	−13.17	−13.64	−14.52			1	
Mrk 1058	9.12	−10.62	−13.25	−14.40				1	
Mrk 1066	8.51	−9.40	−12.62	−13.26				1	
Mrk 1073	6.31	−9.55	−12.66	−13.55				1	
Mrk 1157	6.02	−10.13	−12.64	−13.64				1	
IC 5063	5.53	−9.47	−12.03	−13.05	−15.11	< −12.05	−10.40	16	27
TOL 0109−383	...	−9.87	−12.38	−13.04	−14.65	−12.08			
TOL 1028−301	...	−10.34	−13.70	−14.70	−14.08				
TOL 1238−364	...	−9.51	−12.74	−13.64					
TOL 1351−375	...	10.55	−12.32	−13.29					
MCG−5-23-16	8.0	...	−12.64	−13.62		−10.69	−10.23	19	9
Fairall 188	...	−9.82	−12.89	−13.96					
ESO 32-G2	...	−10.39	...	...			−10.57		8
ESO 103-G35	12.6	−9.74	...	...		< −10.80	−10.36	20	9

REFERENCES.—(1) Dahari & De Robertis 1988; (2) De Zotti & Gaskell 1985; (3) Ward & Morris 1984; (4) Malkan 1983; (5) Veilleux 1991; (6) Atwood et al. 1982; (7) Pounds et al. 1989; (8) Awaki et al. 1991; (9) Turner & Pounds 1989; (10) Matsuoka et al. 1990; (11) Yaqoob & Warwick 1991; (12) Makino et al. 1993; (13) Piro, Yamauchi, & Matsuoka 1990; (14) Winkler 1992; (15) De Robertis & Osterbrock 1986; (16) Phillips, Charles, & Baldwin 1983; (17) Osterbrock & De Robertis 1985; (18) Veron-Cetty & Veron 1986; (19) Durret & Bergeron 1988; (20) Phillips et al. 1979; (21) Koyama et al. 1989; (22) Awaki 1992; (23) Hanson et al. 1990; (24) Iwasawa et al. 1993; (25) Awaki et al. 1990; (26) Warwick et al. 1989; (27) Koyama et al. 1993.

included in the catalog of Fabbiano, Kim, & Trinchieri (1992). Nine other galaxies in our sample were observed with the *Einstein* IPC, but have no previously published fluxes. We have extracted the fluxes for these sources in the 0.2–4 keV band using a technique similar to that described in Fabbiano et al. (1992). No absorption correction has been applied to the SX fluxes given in Table 1. While absorption may substantially reduce the observed flux in this band, determining an absorption correction is difficult given the poor spectral resolution and S/N of the IPC data.

3.5. *Hard X-Rays (HX) (2–10* keV)

We have restricted our sample to those galaxies with available spectra in the 2–10 keV band, so a correction for the absorbing column can be made. In all cases, the absorbing column was found by fitting a power-law + photoelectric absorption model to the X-ray spectrum. The majority of the measurements are from *EXOSAT* and *Ginga*. Table 1 contains HX fluxes for 20 Seyfert 2 galaxies. Although a HX flux has been reported for NGC 5643 (Awaki 1992), this observation appears to be significantly confused by a nearby Galactic source (R. Mushotzky, private communication) so we have not included it in Table 1. Similarly, the X-ray observations of NGC 6814 appear to be contaminated by a nearby cataclysmic variable star (Madejski et al. 1993), so no HX flux measurement is given for this object.

3.6. *Luminosities*

As the present sample is not flux-limited, we have restricted our interpretation to comparisons in flux space to avoid false correlations produced by distance effects. However, there are obvious benefits to luminosity comparisons. For example, it is not always easy to tell if the nearby galaxy NGC 1068 follows the same correlation as the other Seyfert 2's in the flux-flux diagrams because it is several orders of magnitudes brighter at most energies. From the luminosity-luminosity plot this can be more easily discerned. Thus, we include both flux-flux and luminosity-luminosity versions of every emission property we discuss, but our interpretation is driven by the flux-flux versions. Luminosities are calculated assuming $H_0 = 50$ km s^{-1} Mpc^{-1}, $q_0 = 0$ and correcting for a Virgocentric infall of 300 km s^{-1} as described in Whittle (1992).

4. RESULTS AND DISCUSSION

4.1. *Isotropic Properties*

We will consider three potentially isotropic properties of Seyfert galaxies: far-infrared continuum (IR), [O III] λ5007 line emission ([O III]), and hard (2–10 keV) X-ray continuum (HX). The fourth potential property, radio continuum, has already been extensively examined in the literature (e.g., Ulvestad & Wilson 1989; Giuricin et al. 1990). In the standard model, the IR, [O III], and HX emission occur on different scales and thus probe different areas of the AGN environment. Rapid variability of the HX indicate this emission is produced on small scales. The majority of type 1 objects observed in this band shows little evidence for absorption beyond that expected from the Galactic column density along the line of sight (e.g., Turner & Pounds 1989). In contrast, all Seyfert 2's, with the exception of NGC 1068, exhibit column densities in the range $N_H \sim 10^{22}$–10^{24} cm^{-2} (Awaki et al. 1991; Mulchaey et al. 1992). These columns are expected in the dusty torus model as the HXs pass directly through the torus (Krolik & Lepp 1989). The apparent lack of a large photoelectric cutoff in the HX band for NGC 1068 is usually attributed to the torus being Compton-thick ($N_H \geq 10^{25}$ cm^{-2}; Elvis & Lawrence 1988). Thus, the observed 2–10 keV photons in NGC 1068, which are observed to be constant in time, unlike the HX emission of many Seyfert 1's, are presumably due to a scattered nuclear component, although the circumnuclear starburst may contribute significantly even at these high energies (Wilson et al. 1992). The nondetection of several Seyfert 2's (e.g., Mrk 78, Mrk 573; Awaki et al. 1991) in the HX band may be an indication that these objects, like NGC 1068, have very large columns along the line of sight to the nucleus, but are too far away for a scattered component to be seen. The HXs are apparently viewed directly in the other Seyfert 2 galaxies detected to date. This is supported by evidence for variability on the timescale of days in some objects (Mulchaey et al. 1992). Furthermore, the inferred column densities have remained constant over the last $\sim$15 yr for those type 2 objects with available data (e.g., Mulchaey et al. 1993), consistent with the absorption occurring on scales expected for the dusty torus, although a conglomerate of BLR clouds could equally account for the data. Thus, the HX properties of the Seyfert 2's observed to date are consistent with the dusty torus model.

The origin of the infrared emission in Seyfert galaxies remains controversial. Since the covering fraction of the torus is expected to be large, it intercepts most of the optical–UV–X-ray radiation emitted by the central source, and presumably reemits this energy in the infrared (Krolik & Lepp 1989; Pier & Krolik 1992). Storchi-Bergmann, Mulchaey, & Wilson (1992a) have recently found that for most or all Seyfert 2's with ionization cones, the data are consistent with a thermal origin of the observed infrared emission. Although the torus emission is expected to be essentially isotropic at longer wavelengths, modeling by Pier & Krolik (1992) indicates the IR emission can be significantly anisotropic especially at 12 and 25 μm. This effect is particularly important for Seyferts with very optically thick tori ($N_H \geq 10^{25}$ cm^{-2}).

The similarity between the [O III] λ5007 luminosities of the two types of Seyferts has been used to argue that if dusty tori exist, they must be on scales smaller than the NLR (Dahari & De Robertis 1988). A major uncertainty in this comparison concerns the effects of reddening on the observed line fluxes and the conclusions of Dahari & De Robertis (1988) depend strongly on the form of reddening adopted. Radio-loud quasars appear to be significantly more luminous than powerful radio galaxies in [O III] λ5007 line emission, which has been used to argue against the unification of these two populations (Jackson & Browne 1990). However, Hes, Barthel, & Fosbury (1993) have found that these two classes are equally luminous in the emission line [O II] λ3727 and suggest that the [O III] λ5007 line may have a significant component from the compact nuclear region which is subject to obscuration, at least for these high-redshift objects.

A histogram of the ratio of IR to [O III] λ5007 ([O III]) emission for the two types of Seyferts in our sample is given in Figure 1*a*. As can be seen from that figure, the distributions for the two types are similar. This result is consistent with both forms of emission being isotropic and only small intrinsic differences between these quantities for Seyfert 1's and Seyfert 2's. However, the two distributions are not identical: the Seyfert 2 distribution is broader (see Table 2). An examination of Figure 1*a* suggests the larger variance of the Seyfert 2 distribution is due to an excess of Seyfert 2's with a high value of IR to [O III].

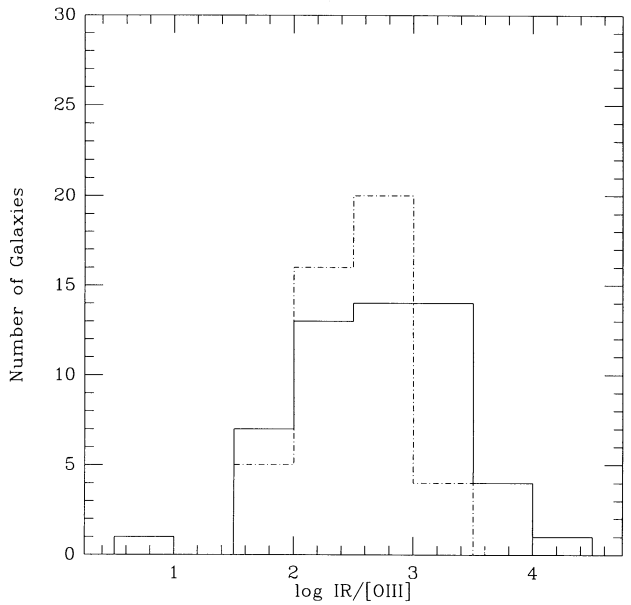

FIG. 1*a*

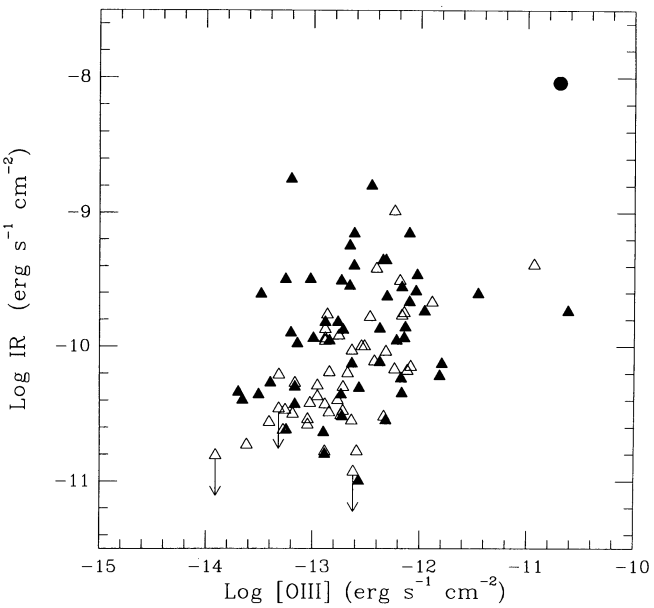

FIG. 1*b*

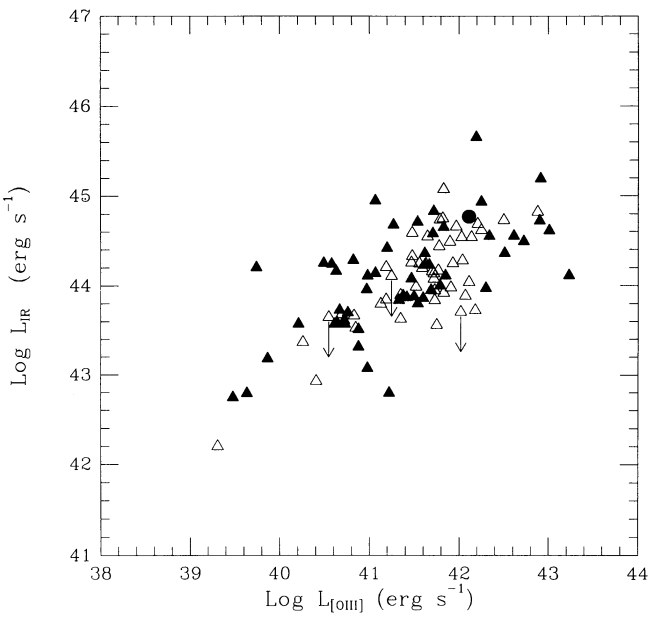

FIG. 1*c*

FIG. 1.—(*a*) Histogram of the logarithm of the ratio of infrared continuum (IR) to [O III] λ5007 ([O III]) for the Seyfert sample in Table 1. Dashed lines represent the Seyfert 1's, solid lines the Seyfert 2's. The distributions for the two Seyfert types are similar, although the Seyfert 2 distribution is broader. (*b*) Plot of IR vs. [O III] emission for the Seyfert sample in Table 1. Open triangles represent the Seyfert 1's, filled triangles the Seyfert 2's. NGC 1068 is represented by a filled circle. There is a correlation between [O III] and IR emission in both Seyfert types, although the relation is much weaker in the Seyfert 2's. (*c*) Same as (*b*), but in luminosity space.

The nature of this excess is such that an additional "warm" component may be present in some Seyfert 2's. A likely candidate is circumnuclear star formation which is known to exist in a significant fraction of Seyfert 2's. Alternatively, the large IR/[O III] ratio in Seyfert 2's could be due to partial obscuration of the [O III] line-emitting regions by the torus, as is implied in radio galaxies (Jackson & Browne 1990). While for the Seyfert 1's there is a strong correlation between the IR and [O III] emission, the relation is much weaker for the type 2 Seyfert's (see Table 3 and Fig. 1*b*). Some of the scatter in Figure 1*b* can probably be attributed to the inclusion of nonnuclear flux in the IR measurements. The presence of a correlation between the [O III] emission, which is presumably produced by photons generated in the active nucleus, and the IR emission suggests the IR must include a component associated with the active nucleus. In fact, the strength of the correlation, particularly in the Seyfert 1's, suggests the nuclear IR component dominates at these energies in many cases.

In Figures 2*a* and 3*a*, a histogram of the ratio of IR and [O III], respectively, (HX) flux is given. In both cases, the distributions for the two types of Seyferts are similar. However, there does not appear to be a tight correlation between either of these quantities and HX (see Figs. 2*b*, 3*b*, and Table 3). The usefulness of these plots is limited by the small number of objects with HX spectroscopy, but the scatter could be due to the large aperture size of *IRAS* and reddening of the observed [O III] fluxes. NGC 1068 has a particularly low ratio of both HX/IR and HX/[O III]. This result is expected if the observed HXs are due to a scattered nuclear component. In this case, we expect the observed HXs to be only a small fraction of the true HX luminosity, while most of the IR and [O III] luminosities are seen. Adopting the boost factor implies from ionization and spectropolarimetric arguments (i.e., ~100; Baldwin, Wilson, & Whittle 1987; Miller, Goodrich, & Mathews 1991; Pier et al. 1994), and applying this to the observed HX flux moves NGC 1068 to a location in Figures 2*a* and 3*a* that is consistent with the other Seyfert 2's {i.e., log (IR/HX) ~ 1.3 and log ([O III]/HX) ~ −1.4}.

We find no evidence for two Seyfert 2 populations in IR, [O III], or HX emission. The HX sample may be strongly biased against "true" Seyfert 2's, since such objects would presumably be very weak at high energies (the weak optical–UV–X-ray continuum in a "true" Seyfert 2 could be intrinsic and not due to obscuration or viewing angle effects). Further-

TABLE 2

DISTRIBUTION PROPERTIES

QUANTITY (1)	FIGURE (2)	SEYFERT 1 Mean (3)	SEYFERT 1 Variance (4)	SEYFERT 2 Mean (5)	SEYFERT 2 Variance (6)	D (7)	K-S TEST PROBABILITY (8)
log (IR/[O III])	1*a*	2.50	0.14	2.70	0.45	0.30	0.02
log (IR/HX)[a]	2*a*	0.57	0.28	0.85	0.21	0.37	0.19
log ([O III]/HX)[a]	3*a*	−1.89	0.25	−1.76	0.38	0.19	0.94
log (UV/SX)	5*a*	−2.93	0.21	−2.56	0.56	0.59	<0.01
log (Hβ/UV)	6*a*	1.24	0.17	1.31	0.35	0.23	0.38
log ([O III]/UV)	7*a*	1.10	0.30	2.21	0.40	0.68	<0.01

Col. (1) Emission quantity being compared; Col. (2) Corresponding figure number; Col. (3) Mean value for Seyfert 1's; Col. (4) Variance in the mean for Seyfert 1's; Col. (5) Mean value for Seyfert 2's; Col. (6) Variance in the mean for Seyfert 2's; Col. (7) Kolmogorov-Smirnov statistic D; Col. (8) Probability that two distributions are drawn from the same population (1.0 = 100% probability).

[a] NGC 1068 not included.

more, most of the Seyfert 2's observed by *Ginga* were selected because they showed broad lines in spectropolarimetry or displayed ionization cones, so there was a strong bias toward "hidden" Seyfert 1's. However, no obvious bias is expected in [O III] and IR. If the present sample does contain two different kinds of Seyfert 2's, these different populations must have remarkably similar energy inputs in these two bands. This would be particularly surprising since the IR emission is most likely dominated by reprocessed optical–UV–X-ray emission, which should be much weaker in the "true" Seyfert 2's. Thus, one would also expect the "true" Seyfert 2's to be much weaker emitters at IR wavelengths. There is no evidence to support the existence of such a population in the present sample.

As noted earlier, much of the scatter in the plots involving infrared emission is probably due to the contributions of nonnuclear sources such as the host galaxy and circumnuclear star-forming regions. Infrared colors can provide a qualitative measurement of the importance of these additional components (Miley, Neugebauer, & Soifer 1985; Rowan-Robinson & Crawford 1989). Figure 4 is a plot of the 100–60 μm spectral index, α(100, 60), against the 60–25 μm spectral index, α(60, 25) for the present sample, where the spectral index α is defined by $f_\nu \propto \nu^\alpha$. A significant fraction of the Seyfert 2's have IR colors similar to those Miley et al. (1985) find for galaxies dominated by normal H II regions. Some of the Seyfert 2's are known to contain circumnuclear star formation (e.g., NGC 1068, NGC 5728, NGC 7582), but little is known about the stellar content of the majority of these galaxies. However, there is a strong correlation between IR color and other indicators of young stars (e.g., radio morphology, presence of infrared polycyclicaromatic hydrocarbon [PAH] features) in many of these galaxies (Wilson 1988), supporting the existence of active star formation in some Seyfert 2's. Ideally, one would like to correct the observed *IRAS* fluxes for the extranuclear contributions. Roche et al. (1991) have measured 12 μm fluxes with small apertures for a handful of Seyferts and find that on average ~60% of the *IRAS* flux at this wavelength in the type 2's can be attributed to the nucleus (compared to ~80% in Seyfert 1's). At longer wavelengths, the host galaxy contribution is probably greater. The relative importance of extranuclear star formation in type 2's compared to type 1's may be due to a selection effect. One possibility is that Seyfert 2's undergoing active star formation are more likely to be detected in the Markarian surveys than a Seyfert 2 without ongoing star formation because of the additional "blue" component. As the majority of Seyfert 2 galaxies are discovered in such surveys, a bias toward star-forming objects might exist. This would also provide a natural explanation for the different ratio of [O III]/60 μm emission Dahari & De Robertis (1988) find for Seyfert 1's and 2's in their Markarian-dominated sample. For current Seyfert samples, it appears that circumnuclear star for-

TABLE 3

CORRELATION STATISTICS FOR FLUX PLOTS

QUANTITY (1)	FIGURE (2)	SEYFERT 1 N (3)	SEYFERT 1 r_s (4)	SEYFERT 1 Probability (5)	SEYFERT 2 N (6)	SEYFERT 2 r_s (7)	SEYFERT 2 Probability (8)
IR vs. O III	1*b*	48	0.63	>0.99	52	0.27	0.94
IR vs. HX	2*b*	17	0.35	0.83	18[a]	0.47	0.85
O III vs. HX	3*b*	17	0.61	>0.99	14[a]	0.14	0.74
SX vs. UV	5*b*	29	0.40	0.97	23	−0.19	0.63
Hβ vs. UV	6*a*	43	0.75	>0.99	25	−0.10	0.38
O III vs. UV	7*a*	43	0.35	0.98	25	0.09	0.34

Col. (1) Emission quantity being compared; Col. (2) Corresponding figure number; Col. (3) Number of data points for Seyfert 1's; Col. (4) Spearman correlation rank for Seyfert 1's; Col. (5) Probability of a correlation for Seyfert 1's (1.00 = 100% probability the two quantities are correlated); Col. (6) Number of data points for Seyfert 2's; Col. (7) Spearman correlation rank for Seyfert 2's; Col. (8) Probability of a correlation for Seyfert 2's (see Col. [5]).

[a] NGC 1068 not included.

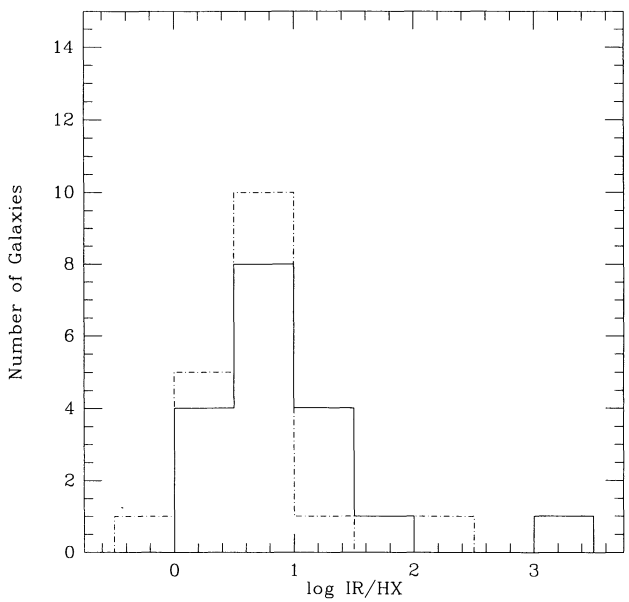

FIG. 2a

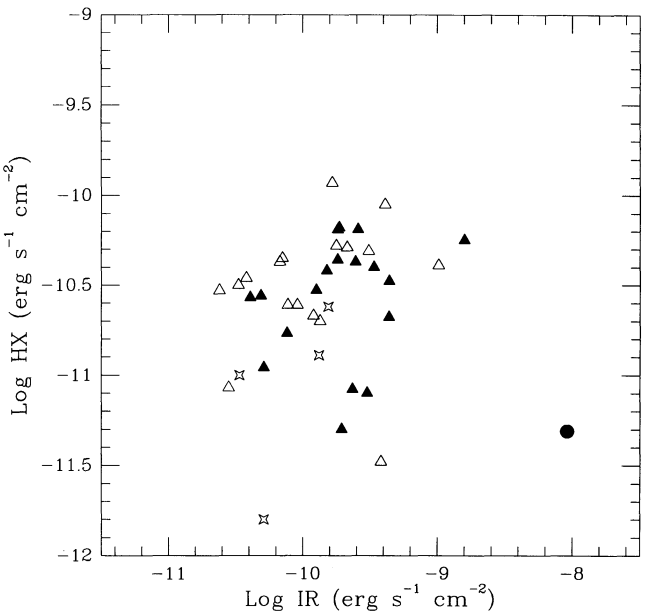

FIG. 2b

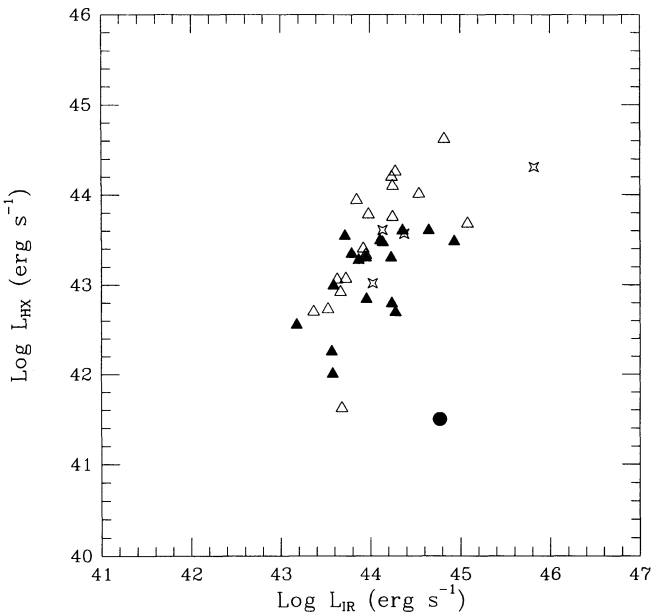

FIG. 2c

FIG. 2.—(*a*) Histogram of the logarithm of the ratio of IR to hard (2–10 keV) X-ray continuum (HX) for the Seyfert sample. Dashed lines represent the Seyfert 1's, solid lines the Seyfert 2's. The hard X-ray fluxes have been corrected for the observed absorbing columns. (*b*) Plot of HX vs. IR emission for the Seyfert sample. Symbols are the same as those used in Fig. 1*b* with the addition of open stars to represent the *IRAS*-selected "Seyfert 2's" observed by *Ginga* (Awaki 1992). (*c*) Same as (*b*), but in luminosity space.

mation is more common in Seyfert 2's than in Seyfert 1's. It will be important to determine if this is due to a selection effect in the current samples or to an intrinsic difference between Seyfert 1's and 2's.

Recently, Awaki (1992) has suggested the existence of a new class of AGN that does not fit in the unified model. Using observations with *Ginga*, he finds that a small sample of Seyfert 2's selected for their high IR luminosities exhibit HX characteristics unlike those of Seyfert 2's selected by other methods. In particular, these *IRAS*–selected objects show no evidence for either strong photoelectric absorption (upper limit of $N_H < 1.5 \times 10^{22}$ cm^{-2}) or Fe Kα line emission, both expected in the dusty torus model. The X-ray spectra of these galaxies tend to be steeper than those of Seyferts ($\alpha = 1.1$–1.3, compared to the canonical value for Seyferts, $\alpha = 0.7$), but possibly consistent with the thermal spectrum expected in a starburst galaxy. However, the HX luminosities of these sources are three orders of magnitude larger than in known starbursts. We include four of these sources along with our Seyfert sample in the plot of IR versus HX (Fig. 2*b*; the fifth source in Awaki (1992) is IRAS 04575−7537 = ESO 33-G2, a previously known Seyfert 2 already in our sample). From this figure it can be seen that the new *Ginga* sources follow the same relation between these quantities as the rest of our sample, implying they may be Seyfert galaxies. However, optical spectroscopy of IRAS 01065−4644 indicates [O III] λ5007/Hβ is less than 1, so it is not a Seyfert 2. Two other objects, IRAS 18325−5926 (Carter 1984) and IRAS 23060+0505 (Hough et al. 1991), have low-ionization spectra intermediate between a Seyfert and a low-ionization nuclear emission-line region (LINER). The IR colors of all of these objects fall in the region where starbursts and Seyfert 2's overlap (see Fig. 4), so the starburst interpretation is still viable. More likely, these galaxies may simply be Seyfert 1's obscured by a few magnitudes of extinction with a significant star formation component also present. This obscuration would be enough to hide the BLR, but not block the HXs. Furthermore, the star formation component would account for low-ionization spectra and IR colors.

4.2. *Anisotropic Properties*

Relative to Seyfert 1's, Seyfert 2's are underluminous in optical, ultraviolet, and SX continuum emission. This result is a natural consequence of the dusty torus model, since the torus is expected to be optically thick to these forms of radiation. Thus, in the simple model, any continuum emission seen in type 2

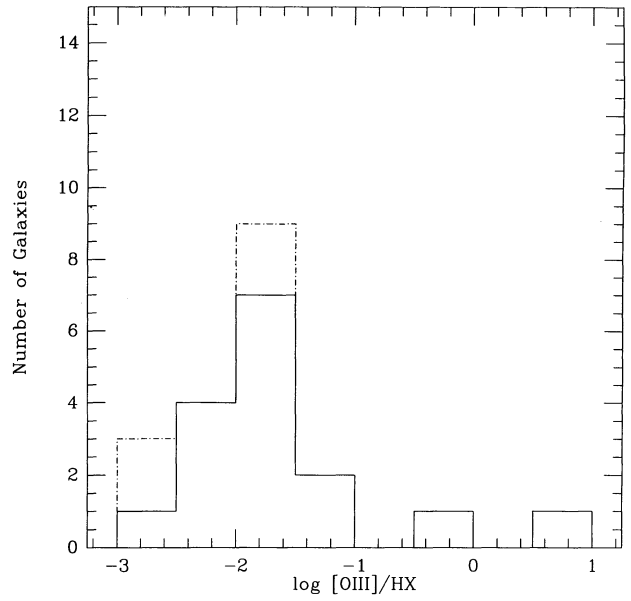

FIG. 3a

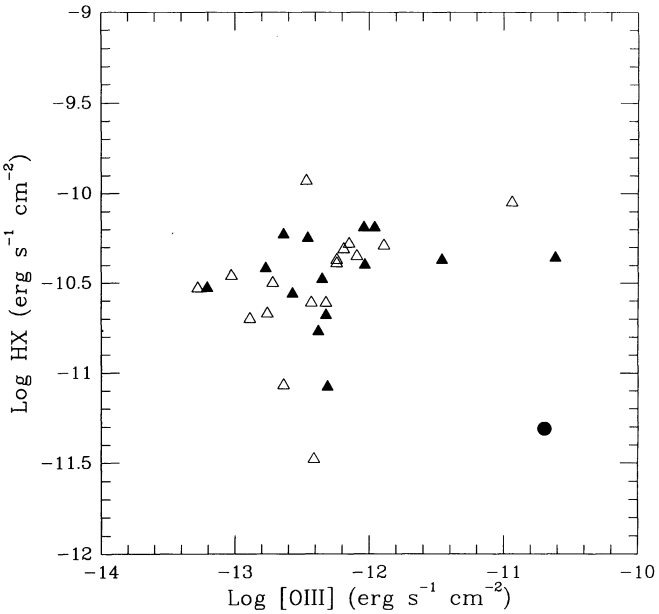

FIG. 3b

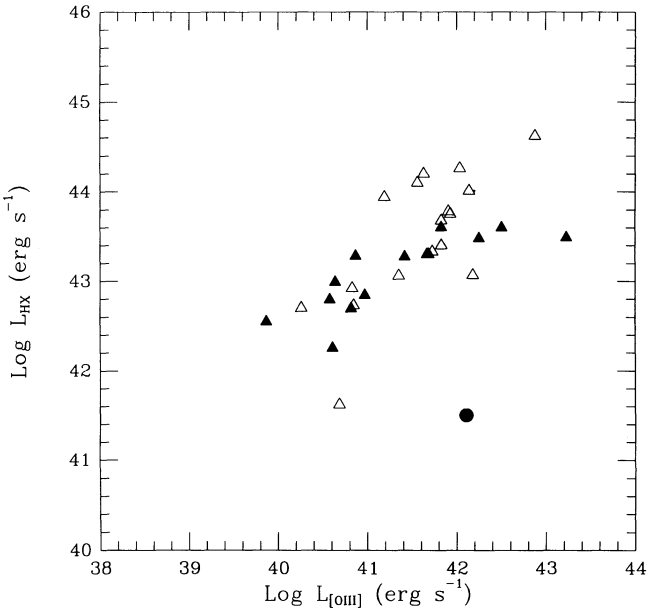

FIG. 3c

FIG. 3.—(*a*) Histogram of the logarithm of the ratio of [O III] to HX for the Seyfert sample. Dashed lines represent the Seyfert 1's, the solid lines the Seyfert 2's. (*b*) Plot of HX vs. [O III] for the Seyfert sample. Symbols are the same as those used in Figs 1*b* and 2*b*. (*c*) Same as (*b*), but in luminosity space.

objects at these wavelengths would presumably be due to either photons scattered into our line of sight or extranuclear sources. The ratio of UV to SX continuum flux is expected to be the same for the two types of Seyferts in a scattering model if the scattering particles are electrons and the scattering region is essentially free of extinction. Masse-Hess et al. (1993) have recently calculated this ratio for a small sample and concluded that it is significantly different for the two types of Seyferts. Figure 5*a* is a histogram of this ratio for our sample. We verify the difference reported by Masse-Hess et al. (1993), although we find considerable overlap of the two distributions and a mean value of UV/SX that is not terribly different (log [UV/SX] ~ -2.93 for the type 1's and ~ -2.56 for the type 2's). Unfortunately, the observed differences of this ratio do not provide a stringent test of the dusty torus model. First, any contribution to the scattering by dust particles will artificially alter this ratio in the Seyfert 2's. While the scattering particles

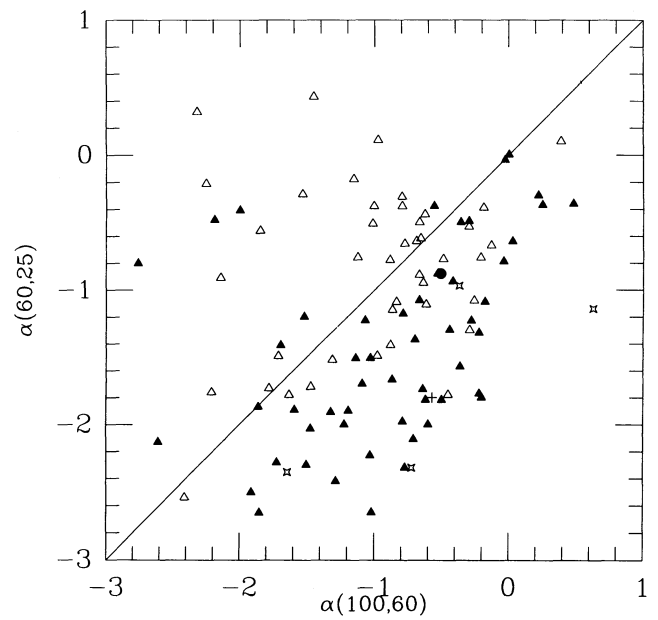

FIG. 4.—Plot of the 60–25 μm spectral index against the 100–60 μm spectral index for the Seyfert sample. Symbols are the same as those used in Figs. 1*b* and 2*b*. The cross marks the mean value of these quantities that Miley et al. (1985) find for H II region galaxies. Note that many of the Seyfert 2's in the present sample have IR colors similar to the H II region galaxies, suggesting a star formation component may contribute a substantial portion of the observed IR emission

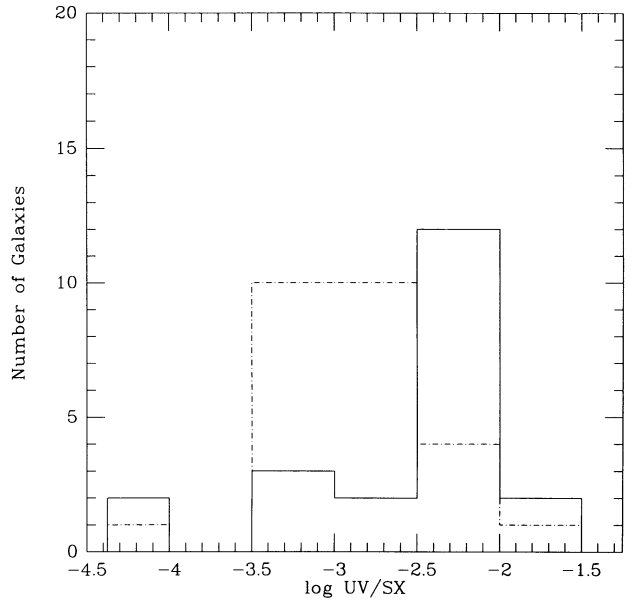

FIG. 5a

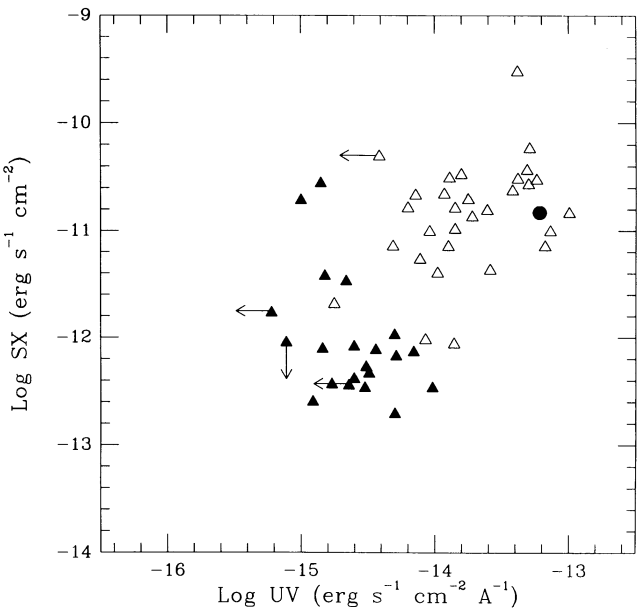

FIG. 5b

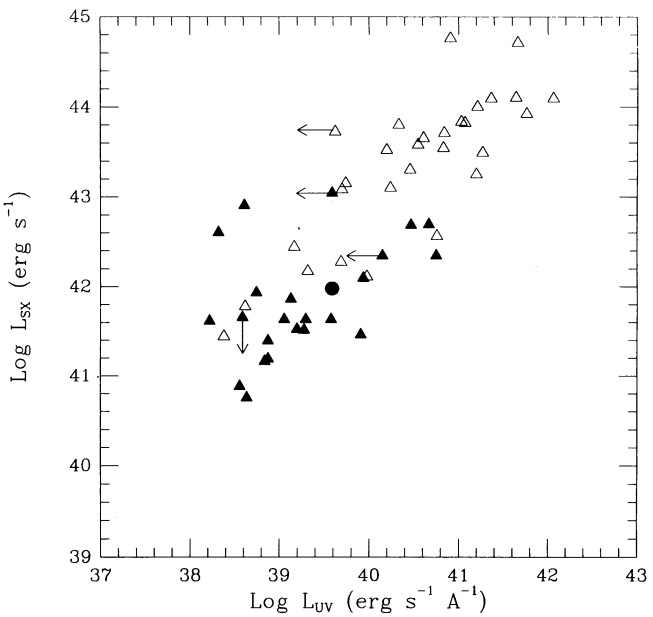

FIG. 5c

FIG. 5.—(*a*) Histogram of the logarithm of the ratio of ultraviolet (UV) to soft (0.2–4 keV) X-ray (SX) continuum emission for the Seyfert sample. Dashed lines represent the Seyfert 1's, solid lines the Seyfert 2's. The distribution of this ratio is different for the two types of Seyferts, as recently claimed by Masse-Hess et al. (1993). (*b*) Plot of SX vs. UV emission for the Seyfert sample. Symbols are the same as those used in Fig. 1*b* (*c*) Same as (*b*), but in luminosity space.

in the *nucleus* of NGC 1068 are essentially confirmed as electrons (see Antonucci 1993), *off-nuclear* scattering by dust is also present in this object (Miller et al. 1991). It seems likely that dust scattering contributes in at least some Seyfert 2's. Furthermore, any obscuring material along the line of sight will change the observed ratio of UV to SX continuum flux, since the UV opacity is dominated by dust, while the X-ray opacity is dominated by gas. For those Seyfert 2's with a relatively low absorbing column to the central source (i.e., $N_H \leq 10^{23}$ cm^{-2}), the "directly viewed" HX continuum contributes substantial flux even at energies as low as 1–2 keV, so the ratio of UV/SX is not a valid test of the scattered nuclear radiation hypothesis in these objects (e.g., NGC 2992, NGC 5506; note the location of these galaxies in Figs. 5*b* and 5*c*). Finally, as both IUE and *Einstein* involved relatively large apertures, contributions from nonnuclear sources such as star formation regions could also lead to a shift of the measured ratio of UV to SX. Thus, in contrast to Masse-Hess et al. (1993), we conclude that the current data do not impose serious constraints on the dusty torus model.

4.3. *Line Emission and the Ionizing Continuum*

Some of the strongest evidence for anisotropy in Seyfert galaxies has come from applying energetic tests to the NLR gas. When a comparison is made between the number of ionizing photons required to produce the line emission and the number of ionizing photons implied from the observed continuum in Seyfert 2 galaxies, a photon deficit is often found. The most plausible explanation for this is that the NLR gas "sees" a stronger ionizing source than we do at Earth (e.g., Wilson et al. 1988; Penston et al. 1990; Kinney et al. 1991a; Storchi-Bergmann et al. 1992b). This could be due to the ionizing source being an intrinsically anisotropic emitter or the ionizing source being obscured from our view by dust.

In Figures 6*b* and 7*b*, we plot the UV continuum versus the total observed Hβ and [O III] fluxes, respectively. For both emission lines (especially Hβ), there is a correlation between line strength and the measured continuum in the Seyfert 1's. The correlation is in the sense, and with the approximate slope, expected for photoionization (cf. Shuder 1981). For the Seyfert 2's, however, there is no significant correlation between these quantities (see Table 3). In the dusty torus model, the observed UV light in Seyfert 2's is scattered, while [O III] and Hβ are dominated by directly viewed emission from the NLR. Since the scattering efficiency, scattering optical depth, and specifics

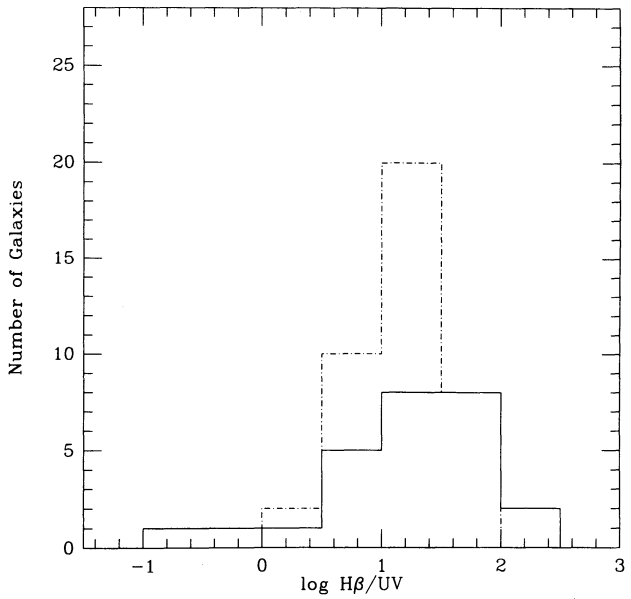

FIG. 6a

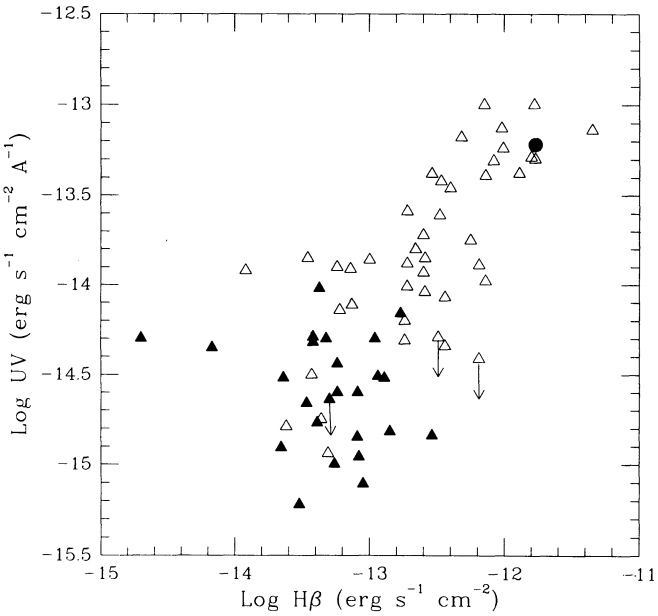

FIG. 6b

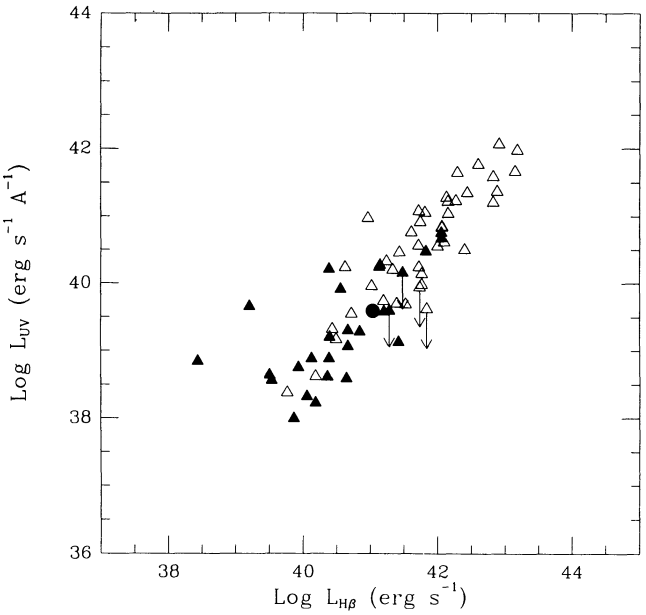

FIG. 6c

FIG. 6.—(*a*) Histogram of the logarithm of the ratio of total Hβ line emission flux to ultraviolet (UV) continuum flux for the Seyfert sample. Dashed lines represent the Seyfert 1's, solid lines the Seyfert 2's. (*b*) Plot of UV vs. total Hβ emission for the Seyfert sample. Symbols are the same as those used in Fig. 1*b*. While there is a fairly strong correlation between these two quantities for Seyfert 1's, there is no apparent correlation in the type 2 Seyferts. (*c*) Same as (*b*) but in luminosity space.

of the scattering geometry are expected to vary significantly among Seyfert 2's, the scatter in the plot of observed UV emission versus narrow-line emission is not surprising. However, the ratio of Hβ/UV is remarkably similar for the two Seyfert types (see Fig. 6*a* and Table 2). This result is not expected or easily explained in the simplest version of the dusty torus model.

The average scattering fraction for Seyfert 2's can be estimated from the plot of UV versus [O III], if we assume the [O III] emission is isotropic (see § 4.1). An examination of Figure 7*b* shows that the Seyfert 2's are on average an order of magnitude fainter in the UV than the Seyfert 1's with similar [O III] luminosities. This suggests a scattering fraction of ~0.1. This number is likely a upper limit, however, since the Seyfert 2's with UV detections are probably brighter in the UV than typical Seyfert 2's, while the Seyfert 1's in the plot should be more representative of their class. As noted earlier, some of the Seyfert 2's are also known to contain substantial starbursts. These additional components probably contribute substantially to the *IUE* fluxes, while producing relatively little [O III] emission. These two effects, among others, suggest an upper limit on the average scattering fraction in Seyfert 2's of ~10%.

5. SUMMARY AND CONCLUSIONS

From our multiwavelength analysis of a large sample of Seyfert galaxies we find the following.

1. The distribution of the ratios of IR/[O III], IR/HX, and [O III]/HX are similar for Seyfert 1's and Seyfert 2's, consistent with the emission in these wavebands being isotropic. However, there is not a strong correlation between any of these quantities for Seyfert 2's, implying substantial contributions in the IR from other sources (e.g., star formation) and strong reddening of the NLR in some cases.

2. The distribution of the ratio of UV continuum to SX continuum (UV/SX) is somewhat different for the two Seyfert types. However, this does not provide a strong test of the dusty torus model, since dust scattering, extinction in the host galaxy and scattering region, contributions from extranuclear sources, and direct contribution to SX from X-rays passing directly through the torus can all affect this ratio.

3. There is a correlation between the emission-line flux and the observed UV continuum in Seyfert 1's, as expected if the line emission is powered by the central source. However, there is no such correlation for the type 2 objects. In the torus model,

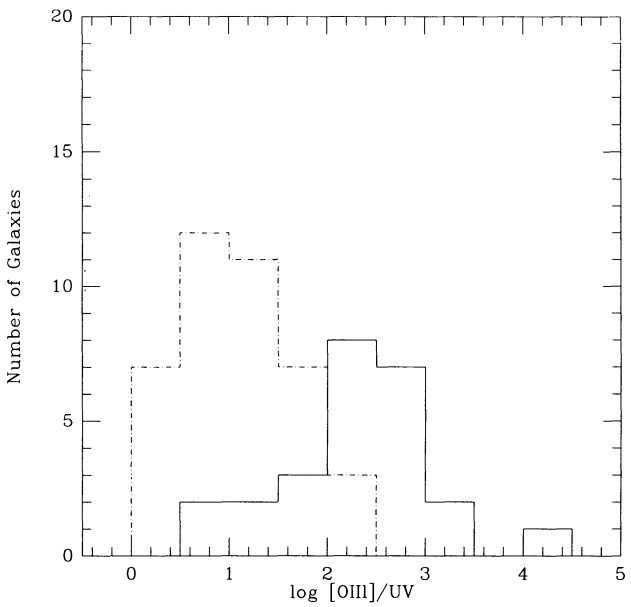

FIG. 7*a*

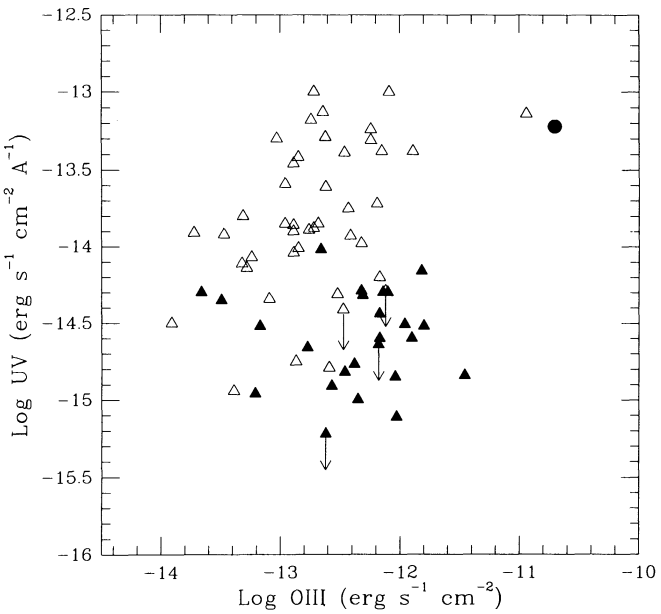

FIG. 7*b*

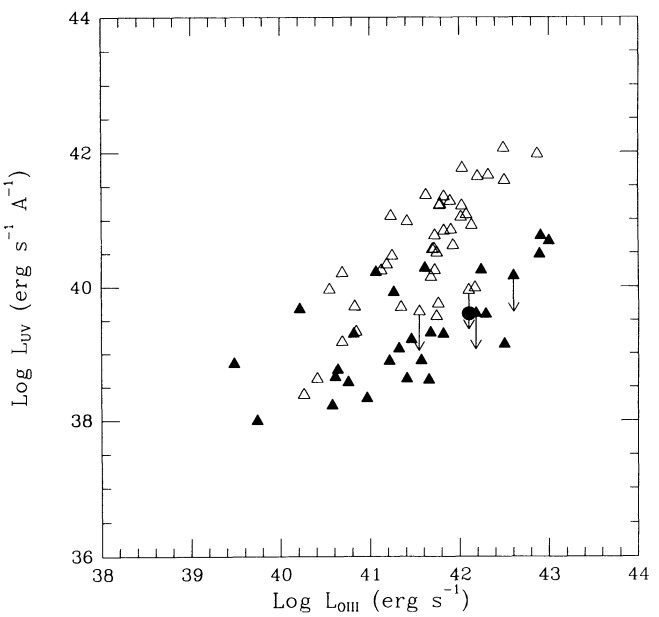

FIG. 7*c*

FIG. 7.—(*a*) Histogram of the logarithm of the ratio of [O III] λ5007 line emission flux to ultraviolet (UV) continuum flux for the Seyfert sample. Dashed lines represent the Seyfert 1's, the solid lines the Seyfert 2's. (*b*) Plot of UV vs. [O III] emission for the Seyfert sample. Symbols are the same as those used in Fig. 1*b*. There is a correlation between the line emission and the UV continuum in the type 1 objects, but no correlation for the type 2's. (*c*) Same as (*b*), but in luminosity space.

this latter result is expected, because the UV is apparently scattered, while the line emission is dominated by a directly viewed component. A scattering fraction of ~10% is required to bring the UV fluxes of Seyfert 2's to a level comparable to Seyfert 1's. This number likely represents an upper limit for the general population of Seyfert 2's, since the present sample is probably biased toward UV-bright Seyfert 2's, and other sources probably contribute to the UV emission in some type 2 objects.

In summary, we find that the continuum and line emission properties of this sample of Seyfert galaxies are generally consistent with the dusty torus model. If there are really two types of Seyfert 2's, obscured Seyfert 1 nuclei and "true" Seyfert 2's (i.e., those with no BLR), a bimodal distribution might be expected in some of the emission properties. We find no evidence for such a distribution in the present sample, but a final answer will probably require the use of larger samples without the selection effects inherent in the current catalogs of known Seyferts.

This project was possible because of the excellent archiving of NASA space-based data. In particular, we are grateful for assistance given at IPAC, NASA/GSFC, and SAO. The NED database was used extensively for this project. We acknowledge useful discussions with Richard Mushotzky, Ed Pier, Thaisa Storchi-Bergmann, and Megan Urry. This research was supported in part by NASA grants NAG 5-1730, NAGW-2689, and NAGW-3268. J. S. M. acknowledges support from a STScI graduate student fellowship.

REFERENCES

Acosta-Pulido, J. A., Perez-Fournon, I., Calvani, M., & Wilson, A. S. 1990, ApJ, 365, 119
Antonucci, R. 1993, ARA&A, 31, 473
Antonucci, R. R. J., & Miller, J. S. 1985, ApJ, 297, 621
Atwood, B., Baldwin, J. A., & Carswell, R. F. 1982, ApJ, 257, 559
Awaki, H. 1992, in Frontiers of X-Ray Astronomy, ed. K. Koyama (Nagoya: Nagoya University), 537
Awaki, H., Koyama, K., Inoue, H., & Halpern, J. P. 1991, PASJ, 43, 195
Awaki, H., Koyama, K., Kunieda, H., & Tawara, Y. 1990, Nature, 346, 544
Baldwin, J. A., Wilson, A. S., & Whittle, D. M. 1987, ApJ, 319, 84
Carter, D. 1984, Astron. Express, 1, 61
Dahari, O., & De Robertis, M. M. 1988, ApJS, 67, 249
De Robertis, M. M., & Osterbrock, D. E. 1986, ApJ, 301, 98
De Zotti, G., & Gaskell, C. M. 1985, A&A, 147, 1

Elvis, M., & Lawrence, A. 1988, ApJ, 331, 161
Evans, I. N., Ford, H. C., Kinney, A. L., Antonucci, R. R. J., Armus, L., & Caganoff, S. 1991, ApJ, 369, L27
Fabbiano, G., Kim, D.-W., & Trinchieri, G. 1992, ApJS, 80, 531
Filippenko, A. V., & Halpern, J. P. 1984, ApJ, 285, 458
Giuricin, G., Mardirossian, F., Mezzetti, M., & Bertotti, G. 1990, ApJS, 72, 551
Green, P. J., Anderson, S. F., & Ward, M. J. 1992, MNRAS, 254, 30
Haniff, C. A., Wilson, A. S., & Ward, M. J. 1988, ApJ, 334, 104
Hanson, C. G., Skinner, G. K., Eyles, C. J., & Willmore, A. P. 1990, MNRAS, 242, 262
Hes, R., Barthel, P. D., & Fosbury, R. A. E. 1993, Nature, 362, 326
Hough, D. H., et al. 1991, ApJ, 372, 478
Iwasawa, J., et al. 1993, in preparation
Jackson, N., & Browne, I. W. A. 1990, Nature, 343, 43
Keel, W. C., de Grijp, M. H. K., Miley, G. K., & Zheng, W. 1994, AJ, in press
Kinney, A. L., Antonucci, R. R. J., Ward, M. J., Wilson, A. S., & Whittle, M. 1991a, ApJ, 377, 100
Kinney, A. L., Bohlin, R. C., Calzetti, D., Panagia, N., & Wyse, R. F. G. 1993, ApJS, 86, 5
Kinney, A. L., Bohlin, R. C., & Neill, J. D. 1991b, PASP, 103, 665
Koyama, K., Inoue, H., Tanaka, Y., Awaki, H., Takano, S., Ohashi, T., & Matsuoka, M. 1989, PASJ, 41, 731
Koyama, K., et al. 1993, in preparation
Krolik, J. H., & Lepp, S. 1989, ApJ, 347, 179
Kruper, J., Urry, C. M., & Canizares, C. R. 1990, ApJS, 74, 347
Lawrence, A. 1987, PASP, 99, 309
Madau, P. 1988, ApJ, 327, 116
Madejski, G. M., et al. 1993, Nature, 365, 626
Makino, F., et al. 1993, in preparation
Malkan, M. A. 1983, ApJ, 264, L1
Masse-Hess, J. M., et al. 1994, ApJ, submitted
Matsuoka, M., Piro, L., Yamauchi, M., & Murakani, T. 1990, ApJ, 361, 440
Miley, G. K., Neugebauer, G., & Soifer, B. T. 1985, ApJ, 293, L11
Miller, J. S., & Goodrich, R. 1990, ApJ, 355, 456
Miller, J. S., Goodrich, R., & Mathews, W. G. 1991, ApJ, 378, 47
Mulchaey, J. S., Colbert, C., Wilson, A. S., Mushotzky, R. F., & Weaver, K. A. 1993, ApJ, 414, 144
Mulchaey, J. S., Mushotzky, R. F., & Weaver, K. A. 1992, ApJ, 390, L69
Osterbrock, D. E. 1989, Astrophysics of Gaseous Nebulae and Active Galactic Nuclei (Mill Valley: University Science Books)
Osterbrock, D. E., & De Robertis, M. M. 1985, PASP, 97, 1129
Penston, M. V., et al. 1990, A&A, 236, 53
Phillips, M. M. 1979, ApJ, 227, L121
Phillips, M. M., Charles, P. A., & Baldwin, J. A. 1983, ApJ, 266, 485
Pier, E. A., & Krolik, J. H. 1992, ApJ, 401, 99
Pier, E. A., Antonucci, R., Hurt, T., Kriss, G., & Krolik, J. 1994, ApJ, submitted
Piro, L., Yamauchi, M., & Matsuoka, M. 1990, ApJ, 360, L35
Pogge, R. W. 1989, ApJ, 345, 730
Pounds, K. A., Nandra, K., Stewart, G. C., & Leighly, K. 1989, MNRAS, 240, 769
Roche, P. F., Aitken, D. K., Smith, C. H., & Ward, M. J. 1991, MNRAS, 240, 838
Rowan-Robinson, M., & Crawford, J. 1989, MNRAS, 238, 523
Shuder, J. M. 1981, ApJ, 244, 12
Storchi-Bergmann, T., Bica, E., & Pastoriza, M. G. 1990, MNRAS, 245, 749
Storchi-Bergmann, T., Mulchaey, J. S., & Wilson, A. S. 1992a, ApJ, 395, L73
Storchi-Bergmann, T., Wilson, A. S., & Baldwin, J. A. 1992b, ApJ, 396, 45
Tadhunter, C., & Tsvetanov, Z. 1989, Nature, 341, 422
Tran, H. D., Miller, J. S., & Kay, L. E. 1992, ApJ, 397, 452
Turner, T. J., & Pounds, K. A. 1989, MNRAS, 240, 833
Ulrich, M. H., et al. 1991, ApJ, 382, 483
Ulvestad, J. S., & Wilson, A. S. 1984, ApJ, 285, 439
———. 1989, ApJ, 343, 659
Veilleux, S. 1991, ApJ, 369, 331
Veron-Cetty, M.-P., & Veron, P. 1986, A&AS, 66, 335
Ward, M., & Morris, S. 1984, MNRAS, 207, 867
Warwick, R. S., Koyama, K., Inoue, H., Takano, S., Awaki, H., & Hoshi, R. 1989, PASJ, 41, 739
Whittle, M. 1992, ApJS, 79, 49
Wilson, A. S. 1988, A&A, 206, 41
Wilson, A. S., Elvis, M., Lawrence, A., & Bland-Hawthorn, J. 1992, ApJ, 391, L75
Wilson, A. S., Ward, M. J., & Haniff, C. A. 1988, ApJ, 334, 121
Winkler, H. 1992, MNRAS, 257, 677
Yaqoob, T., & Warwick, R. S. 1991, MNRAS, 248, 773